Mon. Not. R. astr. Soc. (1982) **200**, 361–375

M/L and velocity anisotropy from observations of spherical galaxies, or must M87 have a massive black hole?

James Binney* and Gary A. Mamon *Princeton University Observatory, Peyton Hall, Princeton, New Jersey 08544, USA*

Received 1981 December 7; in original form 1981 September 7

Summary. An algorithm is developed that determines whether a given set of photometric and spectroscopic observations of a spherical galaxy are consistent with the mass-to-light ratio in the galaxy being constant. If such a model is possible, the value of the mass-to-light ratio and the values of the two independent components of velocity dispersion at each radius are determined. Tests of the algorithm demonstrate its consistency and accuracy when applied to pseudo-data generated from a variety of theoretical models. When the data do not extend to very great radii and must be extrapolated arbitrarily, qualitatively correct results are obtained.

The algorithm is applied to M87. The deconvolution technique of Lucy (1974) is used to correct the photometry of Young *et al.* (1978) for the effects of seeing and a point light source. Velocity dispersion profiles consistent with the observations of Sargent *et al.* (1978) and of Dressler (1980) combine with the photometry to yield physically plausible models that have constant mass-to-light ratio. $M/L_V = 7.6$ if $A_V = 0.14$ and $D = 16$ Mpc. The models returned by different dispersion profiles all involve a tight star cluster at $r < 100$ pc, in which the velocity dispersion is highly anisotropic towards the outside. The main body of the galaxy, which dominates the light beyond $r = 200$ pc, has only modest velocity dispersion anisotropy. The constant mass-to-light models of M87 discussed here are very different from that proposed by Duncan & Wheeler (1980) in which the velocity dispersion in the main body of the galaxy is extremely anisotropic. We believe it is difficult to modify their model to conform with the observations of M87 at $R > 80''$. The models derived here share important features with those proposed by Gurzadyan & Ozernoi (1980) and by Dressler (1980).

1 Introduction

The precision with which the photometric and kinematic properties of elliptical galaxies can be measured has increased dramatically in recent years. The line-of-sight velocity dispersion in a giant elliptical galaxy may now be measured to an accuracy of order 10 per cent from

*Present address: Department of Theoretical Physics, Keble Road, Oxford OX1 3NP.

the centre to many kpc, and in the most favourable cases the surface brightness of the system may be determined accurately out to radii where the blue surface brightness is less than 1 per cent of sky. Furthermore, the advent of CCD detectors makes it possible to measure the apparent central brightness distributions of these galaxies with sufficiently high signal-to-noise that one may even attempt to eliminate the effects of atmospheric seeing on the distribution of light at the centre.

These excellent new data demand new and more sophisticated methods of analysis than have been used heretofore, for even in cases where the galaxy under investigation may be essentially spherical, the methods of analysis that are currently employed lead to ambiguous results. The case of the E1 galaxy M87 will illustrate this point.

M87 has a sharp cusp of luminosity at its centre, which Sargent *et al.* (1978) suggest is an agglomeration of stars about a massive black hole. In order to test this hypothesis Sargent *et al.* obtained measurements of the line-of-sight velocity dispersion in M87 at radii from R = 1 arcsec to R = 80 arcsec, and combined these data with measurements of the central surface brightness profile of M87 by Young *et al.* (1978) to conclude that the mass contained within a sphere of radius r about the centre of M87 does not diminish with diminishing r nearly as rapidly as does the light generated within such a sphere. Sargent *et al.* suggest that this phenomenon may be understood if a black hole of mass $\simeq 5 \times 10^9 M_\odot$ sits at the very centre of M87.

An important assumption in the analysis of Sargent *et al.* was that the velocity dispersion tensor at all points in M87 is effectively isotropic. Unfortunately there is no empirical or theoretical support for this hypothesis, and Duncan & Wheeler (1980) have argued that if one drops the assumption of isotropic velocity dispersion tensor, the observations of Sargent *et al.* and of Young *et al.* may be satisfactorily understood without invoking any unseen mass at the centre of M87. On the other hand, the very simple Eddington model employed by Duncan & Wheeler assumes at the outset that at large distances from the centre of M87 the tangential component of velocity dispersion vanishes entirely. Evidently this assumption is at least as unrealistic as the assumption of completely isotropic velocity residuals. Furthermore, Simien (1981) has concluded that, Duncan & Wheeler's model notwithstanding, one cannot construct an acceptable model of M87 that does not involve a variable mass-to-light ratio.

This situation has prompted us to re-examine this problem in a general framework. In this paper we show that if one knows the surface brightness and the line-of-sight velocity dispersion of a spherical galaxy as functions of galactocentric radius, one may determine the unique constant mass-to-light ratio with which these data are consistent, independently of any assumption about the degree of velocity anisotropy in the galaxy. In fact, the method we introduce here yields as an *output* the radial dependence of the shape of the velocity ellipsoids in the galaxy. In certain galaxies the anisotropy profile that one obtains in this way may be physically implausible, and for these galaxies one may then conclude that the mass-to-light ratio is not independent of radius. But for other galaxies, including M87, one derives from the observations perfectly reasonable anisotropy profiles under the assumption of radius-independent mass-to-light ratio, so that for these systems the stellar observations cannot be used to suggest that they contain dynamically important quantities of dark matter.

In Section 2 we show how the particular constant mass-to-light ratio and velocity anisotropy profile that are consistent with given observations may be determined from the observations. This section is of a somewhat mathematical nature, and the reader who is interested primarily in practical consequences may pass directly to Section 3, where we describe numerical tests of our algorithm in which pseudo data that derive from King (1966), Michie (1963) and $r^{1/4}$-models are inverted and the results compared with the models.

In Section 4 we apply the method to the observations of Sargent *et al.* and of Young *et al.* of M87. We correct the photometry of Young *et al.* (1978) for the effects of seeing and a point light source at the centre, and then explore the models returned by our algorithm under a variety of plausible hypotheses concerning the radial variation of the line-of-sight velocity dispersion. Models associated with velocity dispersion profiles that lie near the centre of the observationally permitted range are both qualitatively and quantitatively plausible. They are, however, very different from the model advocated by Duncan & Wheeler (1980). We argue that their model cannot be adapted to fit the data beyond $R = 80''$. In the concluding Section 5 we argue that the great merit of our algorithm is the hope it offers of some day proving unambiguously that a given E0 galaxy *does* have a variable mass-to-light ratio. However, our results for M87 suggest that that day is not yet come.

2 The algorithm

We confine ourselves to a discussion of the dynamics of a spherically symmetric galaxy. Symmetry then requires that the velocity ellipsoid at each point in the galaxy must be rotationally symmetric about the radial direction. We denote the two independent principal velocity dispersions σ_r and σ_θ and define the velocity anisotropy parameter β as

$$\beta = \frac{\sigma_r^2 - \sigma_\theta^2}{\sigma_r^2} . \tag{1}$$

With this definition $\beta = 0$ in a galaxy whose velocity dispersion tensor is isotropic.

We assume that the surface brightness $\Sigma(R)$ has been measured at all projected radii R, from the centre of the galaxy out to the radius R_t at which the galaxy's surface brightness goes to zero. The luminosity density $l(r)$ may then be determined from the standard inversion

$$l(r) = -\frac{1}{\pi}\int_r^{R_t} \frac{d\Sigma}{dR}\,\frac{dR}{(R^2 - r^2)^{1/2}} . \tag{2}$$

If we assume that the mass-to-light ratio is some constant A, the mass density is simply

$$\rho(r) = \mathrm{A}\, l(r) . \tag{3}$$

The hydrodynamic equation for a spherical system is

$$\frac{d}{dr}(\rho\sigma_r^2) + \frac{2\beta}{r}\rho\sigma_r^2 = -\rho\frac{4\pi G}{r^2}\int_0^r \rho r^2 dr . \tag{4}$$

In terms of A and l this becomes

$$\frac{d}{dr}(l\sigma_r^2) + \frac{2\beta}{r} l\sigma_r^2 = -\mathrm{A}\frac{l u^2}{r} \tag{5}$$

where

$$u^2(r) = \frac{4\pi G}{r}\int_0^r l r^2 dr \tag{6}$$

is defined such that $\sqrt{\mathrm{A}}u(r)$ is the circular velocity at radius r.

Elementary geometry shows that the line-of-sight velocity dispersion $\sigma_v(R)$ is given by

$$\frac{1}{2}\sigma_v^2(R)\Sigma(R) = \int_R^{R_t} \frac{l(r)\sigma_r^2(r)}{(r^2 - R^2)^{1/2}}\, r dr - R^2\int_R^{R_t} \frac{\beta(r) l(r)\sigma_r^2(r)}{r(r^2 - R^2)^{1/2}}\, dr . \tag{7}$$

If A were known empirically and $\sigma_v(R)$ and $\Sigma(R)$ had been determined observationally, equations (5) and (7) could be regarded as a pair of non-linear integro-differential equations for the two unknown functions $\sigma_r(r)$ and $\beta(r)$. Actually we show that these equations yield both A and the functions $\sigma_r(r)$ and $\beta(r)$, though for the moment we proceed as if A were known *a priori*. Eliminating the product $\beta l\sigma_r^2/r$ between equations (5) and (7) yields

$$\frac{1}{2}\left[\Sigma(R)\sigma_v^2(R) - AR^2\int_R^{R_t}\frac{lu^2}{r}\frac{dr}{(r^2-R^2)^{1/2}}\right] = \frac{1}{2}R^2\int_R^{R_t}\frac{d(l\sigma_r^2)}{dr}\frac{dr}{(r^2-R^2)^{1/2}} + \int_R^{R_t}\frac{l\sigma_r^2}{(r^2-R^2)^{1/2}}\,r dr. \tag{8}$$

When we integrate the last term on the right hand side of this equation by parts and combine the resulting integral with the first integral on the right hand side of the equation, we obtain

$$\frac{1}{2}\left[\Sigma(R)\sigma_v^2(R) - AR^2\int_R^{R_t}\frac{lu^2}{r}\frac{dr}{(r^2-R^2)^{1/2}}\right] = \int_R^{R_t}\frac{3/2R^2 - r^2}{(r^2-R^2)^{1/2}}\frac{d(l\sigma_r^2)}{dr}\,dr. \tag{9}$$

With our assumption that A is known, the left hand side of this equation may be evaluated from the observations. Hence, equation (9) is a linear integral equation for the product $l\sigma_r^2$.

It is convenient to discuss the solution of equation (9) in terms of new variables. Define x, X, g and H by

$$x = r^{-2}, \tag{10a}$$

$$X = R^{-2}; \quad X_t = R_t^{-2}, \tag{10b}$$

$$g(x) = \left[r^4\frac{d}{dr}(l\sigma_r^2)\right]_{r=x^{-1/2}}, \tag{10c}$$

$$H(X) = \left\{\frac{1}{R}\left[\Sigma(R)\sigma_v^2(R) - AR^2\int_R^{R_t}\frac{lu^2}{r}\frac{dr}{(r^2-R^2)^{1/2}}\right]\right\}_{R=X^{-1/2}}. \tag{10d}$$

In terms of these variables equation (9) becomes

$$\int_{X_t}^{X}\frac{3/2x - X}{(X-x)^{1/2}}g(x)dx = H(X). \tag{11}$$

In Appendix A we show that the solution of equation (11) is

$$g(x) = \int_{X_t}^{x}\frac{d^2J}{dy^2}\frac{dy}{y} \tag{12a}$$

where

$$J(y) = \frac{2}{\pi}\int_{X_t}^{y}\frac{H(z)}{(y-z)^{1/2}}\,dz. \tag{12b}$$

We may now determine the mass-to-light ratio A by consideration of the behaviour of $g(x)$ at very large values of x, which correspond by equation (10a) to very small radii r.

Equation (10c) shows g to be r^3 times the logarithmic radial derivative of the stellar 'pressure' $l\sigma_r^2$. One expects the stellar pressure at the very centre of a galaxy that has a finite

central potential to be finite, and a galaxy that does not have a point mass at its centre will normally have a finite central potential even if the central density is very large. (For example a spherical galaxy whose projected surface density obeys the $r^{1/4}$ law has a divergent central density but a finite central potential, Young 1976.) Hence, it is likely that at large x, g diminishes as rapidly as $r^3 = x^{-3/2}$, and we may safely assume that $g(\infty) = 0$. Through equations (12) and (10d) this requirement determines the mass-to-light ratio A. In fact, equation (10d) shows that $H(X)$, and therefore $J(y)$ and $g(x)$ are composed of parts that are independent of A and parts that are proportional to A. Therefore if we write

$$g(x) = g_1(x) - \mathrm{A}g_2(x) = \int_{X_t}^{x} \frac{d^2 J_1}{dy^2}\frac{dy}{y} - \mathrm{A}\int_{X_t}^{x} \frac{d^2 J_2}{dy^2}\frac{dy}{y}, \tag{13}$$

where

$$J_1(y) = \frac{2}{\pi}\int_{X_t}^{y} \left[\frac{\Sigma \sigma_v^2}{R}\right]_{R=z^{-1/2}} \frac{dz}{(y-z)^{1/2}} \tag{14}$$

$$J_2(y) = \frac{2}{\pi}\int_{X_t}^{y} \left[R\int_{R}^{R_t} \frac{lu^2}{r}\frac{dr}{(r^2-R^2)^{1/2}}\right]_{R=z^{-1/2}} \frac{dz}{(y-z)^{1/2}}, \tag{15}$$

we have that

$$\mathrm{A} = \lim_{x\to\infty}(g_1/g_2). \tag{16}$$

In Appendix B we reproduce a demonstration due to S. D. Tremaine that equation (16) may be alternatively derived from the virial theorem. Equation (15) for $J_2(y)$ may be simplified. Writing the inner integral in terms of z and x and inverting the order of integrations it becomes,

$$\begin{aligned} J_2(y) &= \frac{1}{\pi}\int_{X_t}^{y} \frac{lu^2}{x^{1/2}}\int_{x}^{y} \frac{dz}{[(z-x)(y-z)]^{1/2}}\,dx \\ &= \int_{X_t}^{y} \frac{lu^2}{x^{1/2}}\,dx \\ &= 2\int_{y^{-1/2}}^{R_t} \frac{lu^2}{r^2}\,dr. \end{aligned} \tag{17}$$

The asymptotic behaviour of J_1 and J_2 at large y ($J_i \sim y$) are such that for numerical work it is expedient to recast equation (13) in terms of new variables K_1 and K_2 that are defined by

$$K_i(y) = \frac{J_i(y)}{y} \tag{18a}$$

In terms of these functions equation (13) is best written

$$g_i(x) = \frac{dK_i}{dx} + 2\int_{X_t}^{x} \frac{dK_i}{dy}\frac{dy}{y}.\star \tag{18b}$$

★ The temptation to evaluate the integral in this equation by parts should be resisted since this procedure expresses g_i as the small difference of large quantities.

Once g and A have been obtained from equations (14)–(18) it is straightforward to obtain the radial velocity dispersion and the anisotropy parameter β that are required by the observations under the assumption of constant mass-to-light ratio:

$$\sigma_r^2(r) = -\frac{1}{2l}\left[\int_{X_t}^{x} g(x)\sqrt{x}\,dx\right]_{x=r^{-2}} \tag{19}$$

$$\beta(r) = \frac{-1}{2l\sigma_r^2}\left(\mathrm{A}lu^2 + r^{-2}g_{|x=r^{-2}}\right). \tag{20}$$

Table 1 summarizes the key results required by an observer who wishes to analyse his data according to our prescription by listing for each quantity the number of the equation from which that quantity should be evaluated.

3 Tests of the algorithm

We have tested the ability of the equations cited in Table 1 to determine the unique mass-to-light ratio and three-dimensional velocity dispersion structure that are consistent with a given set of observations by inverting pseudo-data that had been obtained by projecting one of three theoretical model galaxies on to the plane of the sky. The models we employed were: (1) The King (1966) model that has concentration parameter $c = \log(r_t/r_c) = 2.75$. (2) A Michie (1963) model that is similar to the King model of the first trial excepting that it has a strongly anisotropic velocity dispersion structure in its outer regions. (3) The spherical system whose projected surface density obeys the $r^{1/4}$-law, and whose distribution function is a function of energy only (e.g. Binney 1982). In each case we found that the functions g_1 and g_2 that are defined by equation (13) become accurately constant near the centre, so that the mass-to-light ratio A may be unambiguously determined through equation (16). Furthermore, if the data reach in to one third of the core radius of a King or a Michie model, or

Table 1. Equations from which quantities should be evaluated.

Quantity	σ_r	β	l	u	A	g	g_i	K_i	J_1	J_2
Equation	(19)	(20)	(2)	(6)	(16)	(13)	(18b)	(18a)	(14)	(17)

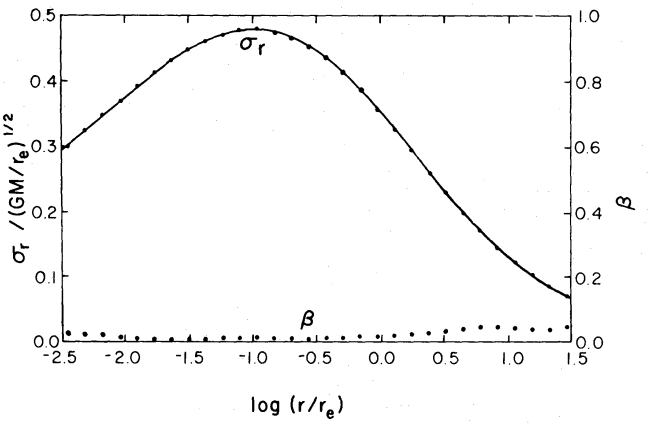

Figure 1. Radial velocity dispersions and anisotropy profiles recovered from pseudo-data generated by the isotropic $r^{1/4}$ model (dotted curves). The solid curve shows the true radial velocity dispersion profile. The anisotropy should of course be zero everywhere.

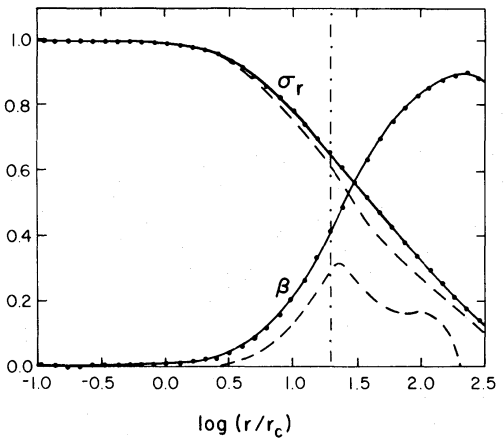

Figure 2. Radial velocity dispersion and anisotropy profiles recovered from pseudo-data generated by a Michie model. The distribution function for this model is $f(E, J) \sim (\exp E - 1) \exp[-(0.05J)^2]$, where E, which is the binding energy with respect to the tidal radius, can take a maximum value of 8.53 and the constant of proportionality is chosen such that the model's central density is $9/4\pi$. The dotted curves are the profiles returned by the algorithm while the solid curves are the true profiles. The dashed curves represent the profiles recovered by pseudo-data generated by this same Michie model out to $r = 20r_c$ (dashed-dotted line) and an isotropic $r^{1/4}$ model beyond.

within a tenth of the effective radius of the $r^{1/4}$-model, the values obtained in this way from the projected data agree with the true values to within the computational errors ($\lesssim 3$ per cent) that attach to the pseudo-data. Figs 1 and 2 show the true and inferred velocity dispersion and anisotropy profiles of two of the models – the agreement between these quantities is even better in the case of the King model than for the models shown here.

Whilst surface photometry may be available for a galaxy down to very low surface brightness levels, the velocity dispersion data cannot be expected to extend much beyond the region where the surface brightness is five or six magnitudes below its peak level. Therefore one will in practice be obliged to extrapolate the data in some fairly arbitrary way. We have tested the stability of our results to such an extrapolation by making up a pseudo-data set by smoothly joining the pseudo-data set of the Michie model of Fig. 2 to the pseuod-data set of a suitably scaled $r^{1/4}$-model like that shown in Fig. 1. The surface density of the Michie model at the joining radius, $r = 20r_c$, is 6.4 mag below the central value and the effective radius of the $r^{1/4}$-profile is $r_e = 10r_c$. The dotted curves in Fig. 2 show the anisotropy and σ_r profiles returned. One sees that the algorithm correctly detects the anisotropy of the Michie model, even though the anisotropy is somewhat masked when the data are completed with the profiles of the isotropic $r^{1/4}$-model. However, the discontinuity in the gradient of β at the matching radius is clear enough, and in a practical case would suggest that one complete the data with the profiles of an anisotropic model. This would tend to restore the original excellent fit between the true and the inferred quantities.

4 Application to M87

4.1 ADOPTED SURFACE BRIGHTNESS PROFILE

The V-band photometry reported by Young *et al.* (1978) has a very high signal-to-noise ratio, which enables one to deconvolve the data for the effects of seeing. We have used the iterative deconvolution technique described by Lucy (1974) to estimate the true surface brightness profile. Appendix C gives some details of the application of this method to the

surface brightness profiles of round galaxies. We adopt a three component Gaussian point spread function (PSF) of the type advocated by Brown (1974) and by de Vaucouleurs & Nieto (1979). The central component of this PSF has the same dispersion $\sigma_1 = 0''.46$ as that used by Young *et al.* The outer components, each of which accounts for 7 per cent of the total light, have dispersions $\sigma_2 = 2\sigma_1$ and $\sigma_3 = 4\sigma_1$.

The trial solutions from which we started the iterations called for by Lucy's algorithm are sums of the raw data and a point source at the centre. We find that after a few iterations trial solutions of this form are transformed into smooth surface brightness profiles that convolve with the adopted PSF to apparent surface brightness distributions that everywhere fit the data to better than 0.05 mag.

The true surface brightness profile that we obtain in this way does depend on the apparent magnitude of the point source in the trial solution from which we started. However, we have found that the only true brightness distributions that invert via equation (2) to luminosity densities $l(r)$ that are monotone functions of r are those that involve point sources whose apparent magnitudes lie in the range $16.85 < V < 16.9$. We have adopted $V = 16.88$ which yields the apparent profile shown in Fig. 3. Fig. 5(a) shows the corresponding luminosity density. The black hole model of Young *et al.* involves a point source of magnitude $V = 16.69$, and the model of M87 of published by Duncan & Wheeler (1980) assumes $V = 16.0$.

The photometry of Young *et al.* does not extend beyond $R = 80''$, where the surface brightness is 5.2 mag below its peak value. Photometry of the outer regions of M87 has been published by Liller (1960), de Vaucouleurs (1969), Oemler (1976), Kormendy (1977), King (1978), Carter & Dixon (1978) and others, but inspection of fig. 1 of Carter & Dixon (1978) shows that beyond $R = 200''$ there is considerable scatter between the results of different observers. The profile may be fitted to within this scatter by an $r^{1/4}$-profile that has $R_e = 105''$ and $\mu_v(R_e) = 21.91$. We have used this profile to extend the data of Young *et al.* down to very low light levels.

4.2 ADOPTED VELOCITY DISPERSION PROFILE

Fig. 4 shows the data of Sargent *et al.* (1978) and the innermost point of Dressler (1980) for an assumed distance to M87 of 16 Mpc. It is clear that $\sigma_v(R)$ is considerably less well deter-

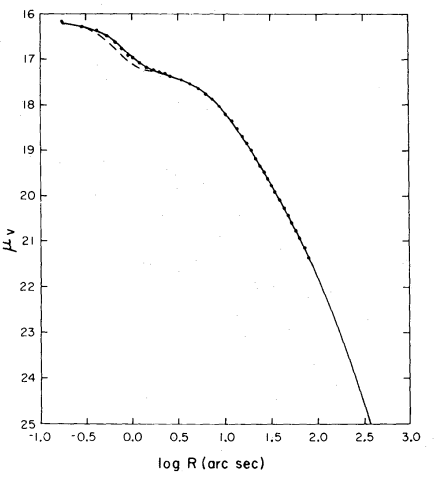

Figure 3. Surface brightness profiles for M87. The dots are the observations by Young *et al.* (1978). The dashed curve shows the true surface brightness profile adopted here. The solid curve shows the result of convolving this profile through a three component PSF after addition of a central point light source, $V = 16.88$.

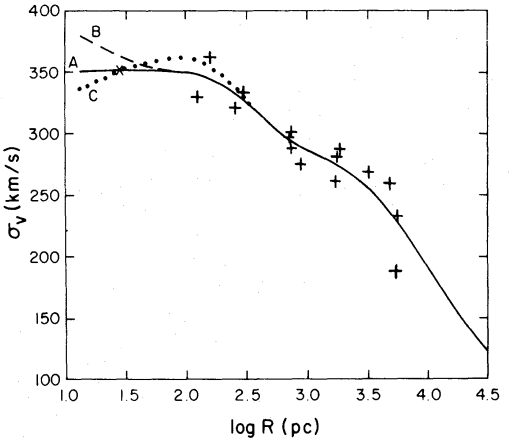

Figure 4. Projected velocity dispersion profiles for M87. The plus signs show the measurements of Sargent *et al.* (1978) and the cross is a measurement by Dressler (1980). Three adopted profiles, are shown. The abscissa was transformed to parsecs using a distance to M87 equal to 16 Mpc (1″ = 77.6 pc).

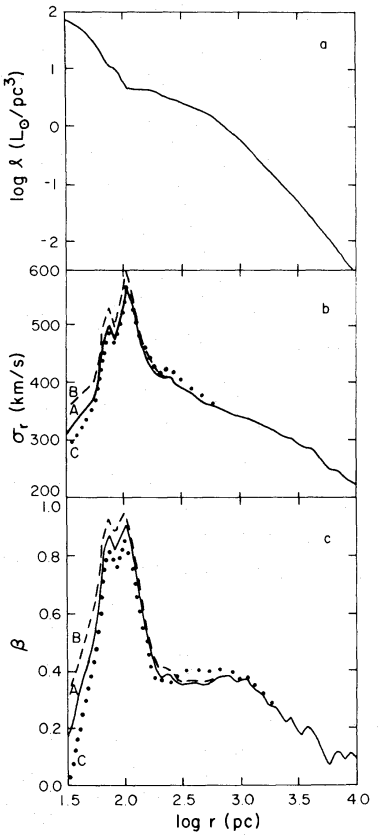

Figure 5. Computed profiles for the luminosity density (a), the radial velocity dispersion (b), and the anisotropy (c) in M87. The luminosity density scale in the top panel assumes an absorption $A_V = 0.14$. The bottom two panels show computed profiles for the three adopted projected velocity dispersion profiles shown in Fig. 4.

mined than $\Sigma(R)$. Two sources of uncertainty over and above the formal measurement uncertainty should be considered: (1) The seeing may have diminished the gradient of $\sigma_v(R)$ near the centre. (2) The distribution of line-of-sight velocities near the centre cannot be Gaussian. The Fourier quotient program used by Sargent *et al.* to reduce their observations is

known to provide a good estimate of $\langle v^2 \rangle$ when the line-profile is Gaussian, but it seems likely that $\langle v^2 \rangle$ may be underestimated by this program when the wings of the profile are more extensive than those of a Gaussian. Given these uncertainties one must check that one's conclusions do not depend sensitively on the precise velocity dispersion profile adopted. In Fig. 4 we show just three dispersion profiles, but we have explored many other profiles with results that will be described below.

We have extrapolated the dispersion profiles from the measured inner part of M87 to large radii by joining these smoothly to the projected velocity dispersion profile of the $r^{1/4}$-law model whose residuals are isotropic ($\beta = 0$) and whose R_e is that used to extend the photometric profile to large radii. Our results for the well observed central part of M87 are not sensitive to the details of this extrapolation.

4.3 MODELS OF M87

Fig. 5(b) and (c) shows respectively $\sigma_r(r)$ and $\beta(r)$ as computed from the three projected velocity dispersion profiles shown in Fig. 4. The mass-to-light ratio of these three models is $M/L_V = 7.61$ dex $[-0.4(A_V - 0.14)] \pm 0.01$ in solar units. The anisotropy, which is always small at the centre, rises steeply to attain a value of near 0.9 at $r = 100$ pc, falls rapidly to a value of near 0.4 by 200 pc and fluctuates near this value out to 1 kpc. From 1 kpc to the end of the data at 10 kpc, the anisotropy declines slowly towards zero.

The general features of the profiles shown in Fig. 5(b) and (c) are not sensitive to the adopted $\sigma_V(R)$ profile. We have tried many other projected velocity dispersion profiles. Varying $\sigma_V(R)$ by $\pm 10\,\mathrm{km\,s^{-1}}$ for $R \geqslant 1''$ produced remarkably similar results. However, if we vary σ_V at $R_0 = 0''.17$, where the lack of measurements puts little constraint on our choice, the anisotropy profile becomes unphysical ($\beta > 1$) for $\sigma_V(R_0) > 400\,\mathrm{km\,s^{-1}}$, and unrealistic ($\beta < 0$) for $\sigma_V(R_0) < 330\,\mathrm{km\,s^{-1}}$.

The curves shown in Fig. 5 invite interpretation in terms of a simple physical picture that is very similar to those advocated by Gurzadyan & Ozernoi (1980) and Dressler (1980). At the centre of the galaxy there sits a tight star cluster. As in a Michie model, the velocity dispersion tensor in this cluster is isotropic at the centre and strongly anisotropic at radii that are large compared to its very small core radius. At about 100 parsecs the density of the main body of the galaxy begins to be important by comparison with the rapidly decreasing density of the central cluster. The overall density starts to decline less steeply and the anisotropy drops to the value $\beta = 0.4$ that is characteristic of the galaxy as a whole.

An anisotropy of order $\beta = 0.4$ in the main body of the galaxy is not unexpected considering that the halo RR Lyrae stars in our Galaxy have $\beta \approx 0.5$ (Woolley 1978).

The origin of galactic nuclei is very uncertain, but one possibility is that they form from globular clusters whose orbits have decayed through the action of dynamical friction (Tremaine, Ostriker & Spitzer 1975). M87 is even now remarkably well endowed with luminous globular clusters (Hanes 1977); the luminosity $\approx 1.2 \times 10^8 L_\odot$ of the inner 100 pc of M87 is only a quarter of the integrated luminosity of the globular clusters that are counted by Hanes. Thus only a small fraction of the original globular clusters of M87 need to spiral to the centre of the galaxy to account for the luminosity cusp there. Since the clusters observed by Hanes are all luminous ($L \geqslant 4 \times 10^5 L_\odot$) and therefore presumably massive, this does not seem implausible. Once a hyperdense core has formed at the centre of a galaxy, two-body interactions between the stars may lead to some sort of gravithermal runaway (Spitzer & Saslaw 1966). In this picture, which is similar to the standard picture of core collapse in a globular cluster (e.g. Cohn 1979, and references therein), stars that gain energy through encounters in the hyperdense core, accumulate on very elongated orbits. In conse-

quence the nucleus gradually becomes surrounded by an envelope in which the velocity dispersion tensor is highly anisotropic. In fact, Gunn & Griffin (1979) have concluded from measurements of the radial velocities of stars in the globular cluster M3 that this cluster has exactly such a halo of stars on highly elongated orbits. Our model of the central 200 pc of M87 conforms to this picture nicely.

4.4 RELATION TO THE MODEL OF DUNCAN AND WHEELER

Our model of the central portion of M87 is quite unlike those of Sargent *et al.* (1978) and of Duncan & Wheeler (1980; DW). There is no difficulty understanding why we differ from Sargent *et al.*, who chose to set $\beta = 0$ and allow the mass-to-light ratio to vary with radius. But the gulf that separates our model, in which $\beta > 0.8$ only near $r = 100$ pc, and that of DW in which $\beta > 0.9$ for $r > 1.7$ kpc and $\beta > 0.99$ for $r > 5.5$ kpc has to be explained, since the DW model has constant mass-to-light ratio A and our algorithm recovers the *unique* model that has constant A and is compatible with a given set of observations. If the difference between our model and that of DW arises from the relatively minor differences between the observable properties of the two models at $R < 80''$, one could repose little confidence in our model of M87.

DW remark that the velocity dispersion and surface brightness profiles of their Eddington model deviate from the observed properties of M87 at radii in excess of $R = 80''$. In fact beyond this radius the line-of-sight velocity dispersion of their model rises gently and the luminosity density begins to fall off like $l(r) \sim r^{-2}$. At least the luminous component of M87 does not behave like this, so the DW model of the central portion of M87 can be considered acceptable only if it can be joined to an envelope in which the luminosity density falls off as steeply as in M87.

Suppose that one had attached to the DW model at $R = 80''$ an envelope of this type. Then the attraction of the combined mass of the envelope and the inner portion of the DW model would have to be sufficient to halt the outward radial motion of stars at $r = 80''$ by radii comparable to $80''$, because otherwise the radical reduction in the density at radii $r > 100''$ that is involved in replacing the outer portion of the DW model by a more realistic envelope would disturb the structure interior to $80''$. Since the observations require that the density of the envelope be everywhere less than the density of the unmodified DW model, it follows that the DW model can be adapted to conform with the observations of M87 at $r > 80''$ only if a star of the original DW model that had radial velocity $v_r = \sigma_r$ at $r = 80''$ is unable to reach greatly beyond this radius. Actually such a star would not reach apgalacticon before $r = 272''$, and a star that moved with speed $\sqrt{2}\sigma_r$ at $80''$ would reach out to $r =$ 37 arcmin in the DW model. This may be contrasted with the situation of stars that are at comparable radii in a King model resembling M87. A star that has $v_r = \sigma_r$ at $80''$ in such a model will reach apgalacticon at $100''$, and a star that has $v_r = \sqrt{2}\sigma_r$ will reach only to $130''$. Hence while the structure of a star cluster, whose velocity dispersion tensor is fairly isotropic, is reasonably local, the halo of an Eddington model is very non-local and one cannot assume that it can be truncated at an arbitrarily chosen radius. Indeed this discussion suggests that the density of the DW model can be brought down to acceptably low level by $r = 150''$ only by *increasing* the already excessive density between $80''$ and $100''$ so as to provide the additional gravitational attraction required to halt the radial motions of the stars at $r = 80''$.

5 Conclusions

The problem posed by a complete set of spectroscopic and photometric observations of a spherical galaxy is under-determined – of the six functions of radius that are involved in the

problem (σ_v, Σ, ρ, l, σ_r and β) only two (σ_v and Σ) can be determined observationally. Equation (2) linking Σ and l, equation (7) linking σ_v to σ_r and β and equation (5), which imposes dynamical equilibrium, provide only three relations between the remaining four functions. This leaves us with a free choice of the form of one function before we solve for a particular model.

We have developed an algorithm which constructs the unique spherical model galaxy of constant mass-to-light ratio that is compatible with given runs of projected surface brightness and velocity dispersion. The mass-to-light ratio of the model and the radial variation of the two independent components of velocity dispersion are determined. Tests of the algorithm on pseudo-data generated from model galaxies that have different brightness profiles and anisotropy structures demonstrate the reliability of the method. Qualitatively correct results are obtained when data are available only for the central portions of the model and then must be arbitrarily extrapolated to large radii.

This technique will not return a physically acceptable model from any data. The anisotropy parameter β is strictly limited to be less than one, and would normally be expected to exceed zero, indicating that the radial component of velocity dispersion exceeds the tangential component.

We have applied our technique to the photometric and spectroscopic data for M87 of Young *et al.* (1978) and of Sargent *et al.* (1978). We find that when the photometric data are properly corrected for the effects of seeing and of a central point source of light, they yield a monotone decreasing luminosity density only if the magnitude of the central light source lies in the range $16.85 < V < 16.9$. We adopt $V = 16.88$. We continue the luminosity profile beyond the radius attained by the data of Young *et al.* as an $r^{1/4}$-law. The velocity dispersion profile of M87 is rather uncertain. We have tried several plausible profiles and find that our results are qualitatively independent of the profile assumed.

A velocity dispersion profile that lies at the centre of the observationally favoured band yields a very plausible model of M87. The mass-to-light ratio of this model is $M/L_V = 7.61$. The velocity dispersion, which is isotropic very close to the centre of the system, becomes highly anisotropic around $r = 100$ pc. We interpret this rise in the anisotropy as due to the accumulation of stars on highly radial orbits during the formation of the stellar nucleus of M87. Beyond $r = 100$ pc the luminosity profile of M87 flattens off as the main body of the galaxy starts to contribute more light than the nuclear component. The anisotropy profile drops steeply at the same radii until it levels off at the value $\beta \approx 0.4$ characteristic of the body of the galaxy.

Our model does not clarify the nature of the light source which is commonly supposed to sit at the centre of M87. This may be a point source, or a cusp of luminosity whose characteristic scale is much smaller than $0''.46$. Whatever its nature we have assumed that the mass associated with it may be neglected. If the mass-to-light ratio of the central source were the same as that of the galaxy as a whole, it would contribute $2 \times 10^8 M_\odot$ to the overall mass or 18 per cent of the mass interior to 100 pc. The effect of including this additional mass would be to diminish the anisotropy in the central regions. However, as Sargent *et al.* have shown, a mass of $5 \times 10^9 M_\odot$ at the centre is required to eliminate the need for anisotropy entirely.

We discuss why our constant mass-to-light model of M87 differs from that suggested by Duncan & Wheeler (1980). We believe that the latter cannot be joined smoothly to an envelope characteristic of the outer regions of M87.

Our recovery of a model of M87 that conforms to the observations without invoking any black hole, does not prove that there is no black hole at the centre of M87. Certainly it is suggestive that the model we recover can be neatly interpreted as a two-component model of the centre of M87, in particular one in which the radial component of velocity dispersion is

everywhere larger than the tangential component. But in the long run the principal value of our algorithm for recovering constant mass-to-light models may be the hope it offers of proving that some set of data is incompatible with constant mass-to-light ratio, because the unique model that is returned by the algorithm from the data involves $\beta > 1$.

Acknowledgments

We thank J. Goodman for help with equation (11) and G. de Vaucouleurs, J. P. Ostriker and S. D. Tremaine for critical readings of the manuscript. GAM acknowledges the National Science Foundation for support under grant AST 78-23796.

References

Binney, J., 1982. *Mon. Not. R. astr. Soc.*, in press.
Brown, G. S., 1974. *University of Texas Publ. Astr.* No. 11.
Carter, D. & Dixon, K. L., 1978. *Astr. J.*, **83**, 574.
Cohn, H., 1979. *Astrophys. J.*, **234**, 1036.
de Vaucouleurs, G., 1969. *Astrophys. Lett.*, **4**, 17.
de Vaucouleurs, G. & Nieto, J.-L., 1979. *Astrophys. J.*, **230**, 697.
Dressler, A., 1980. *Astrophys. J.*, **240**, L 11.
Duncan, M. J. & Wheeler, J. C., 1980. *Astrophys. J.*, **237**, L27.
Gunn, J. E. & Griffin, R. F., 1979. *Astr. J.*, **84**, 752.
Gurzadyan, V. G. & Ozernoi, L. M., 1980. *Soviet Astr. Lett.*, **6**, 75.
Hanes, D. A., 1977. *Mem. R. astr. Soc.*, **84**, 45.
King, I. R., 1966. *Astr. J.*, **71**, 64.
King, I. R., 1978. *Astrophys. J.*, **222**, 1.
Kormendy, J., 1977. *Astrophys. J.*, **214**, 359.
Liller, M. H., 1960. *Astrophys. J.*, **132**, 306.
Lucy, L. B., 1974. *Astr. J.*, **79**, 745.
Michie, R. W., 1963. *Mon. Not. R. astr. Soc.*, **125**, 127.
Oemler, A., Jr., 1976. *Astrophys. J.*, **209**, 693.
Sargent, W. L. W., Young, P. J., Boksenberg, A., Shortridge, K., Lynds, C. R. & Hartwick, F. D. A., 1978. *Astrophys. J.*, **221**, 731.
Simien, F., 1981. *Thèse de doctorat d'état*, Université de Provence.
Spitzer, L., Jr. & Saslaw, W. C., 1966. *Astrophys. J.*, **143**, 400.
Tremaine, S. D., Ostriker, J. P. & Spitzer, L., 1975. *Astrophys. J.*, **196**, 407.
Woolley, R., 1978. *Mon. Not. R. astr. Soc.*, **184**, 311.
Young, P. J., 1976. *Astr. J.*, **81**, 807.
Young, P. J., Westphal, J. A., Kristian, J., Wilson, C. P. & Landauer, F. P., 1978. *Astrophys. J.*, **221**, 721.

Appendix A: Solution of equation (11)

By analogy with Abel's integral equation, multiply (11) by $(y - X)^{-1/2}$ and integrate over X;

$$\int_{X_t}^{y} \frac{dX}{(y-X)^{1/2}} \int_{X_t}^{X} \frac{(3/2x - X)g(x)}{(X-x)^{1/2}}\, dx = \int_{X_t}^{y} \frac{H(X)\,dX}{(y-X)^{1/2}}\,. \tag{A1}$$

The left-hand side of this equation becomes on a change in the order of integration

$$\int_{X_t}^{y} g(x)\,dx \int_{x}^{y} \frac{(3/2x - X)\,dX}{[(y-X)(X-x)]^{1/2}} = \frac{\pi}{2}\int_{X_t}^{y} g(x)(2x - y)\,dx \tag{A2}$$

where we have evaluated the inner integral with the aid of the substitution $\sin^2\theta = (X-x)/(y-x)$. Substituting (A2) into (A1) and differentiating twice with respect to y we obtain

$$\frac{dg}{dy} = \frac{2}{\pi y}\frac{d^2}{dy^2}\int_{X_t}^{y}\frac{H(X)\,dX}{(y-X)^{1/2}} = -\frac{1}{y}\frac{d^2J}{dy^2}$$

from which equation (12a) follows immediately.

Appendix B: Derivation of equation (16) from the virial theorem

Integrating equation (12a) twice by parts we obtain

$$g_i(\infty) = 4\int_0^{R_t} J_i(r^{-2})\,r^3\,dr. \tag{B1}$$

Substituting for J_1 from equation (14) we have,

$$g_1(\infty) = \frac{16}{\pi}\int_0^{R_t} r^4\,dr\int_0^{R_t}\frac{\Sigma\sigma_v^2}{R^3}\frac{dR}{(R^2-r^2)^{1/2}} \tag{B2}$$

and upon changing the order of integration this becomes,

$$g_1(\infty) = 3\int_0^{R_t}\Sigma(R)\,\sigma_v^2\,R\,dR = \frac{T}{\pi A} \tag{B3}$$

where T is the total kinetic energy of the galaxy.

From equations (B1) and (17) we have that

$$g_2(\infty) = 8\int_0^{R_t}\int_r^{R_t}\frac{lu^2}{R^2}\,dR\,r^3\,dr. \tag{B4}$$

On exchanging the order of integration in equation (B4) and substituting from equation (6) for u^2 we obtain

$$g_2(\infty) = \frac{G}{2\pi A^2}\int_0^{R_t}\frac{M\,dM}{r} = \frac{|W|}{2\pi A^2}, \tag{B5}$$

where W is the total potential energy of the system. Equation (16) now follows from the ratio of equations (B3) and (B5) and the virial theorem.

Appendix C: Correction of photometry of a circular galaxy for seeing

Let $\phi(R)dR$ be the probability that a photon is received in some interval of time Δt in an annulus of the sky of mean radius R, and $\psi(R)dR$ be the corresponding probability that a photon is emitted into this annulus. Suppose, furthermore, that $P(R|R')dR$ is the probability that a photon that is emitted at radius R' is scattered by the seeing into the annulus centred on R. Then

$$\phi(R) = \int_0^{\infty}\psi(R')\,P(R|R')dR', \tag{C1}$$

and Lucy (1974) shows that $\psi(R)$ is approached by the sequence of functions $\psi_n(R)$ that are defined by

$$\psi_{n+1}(R') = \psi_n(R) \int_0^\infty \frac{\phi(R)}{\phi_n(R)} P(R|R')dR \tag{C2}$$

$$\phi_n(R) = \int \psi_n(R') P(R|R')dR' \tag{C3}$$

for any reasonable choice of ψ_0.

If the point spread function is a single Gaussian of dispersion σ,

$$P(R|R')dR = \frac{1}{2\pi\sigma^2} \int_{|\mathbf{R}|=R} \exp\left[\frac{-|\mathbf{R}-\mathbf{R}'|^2}{2\sigma^2}\right] d^2\mathbf{R}$$

$$= \frac{1}{\pi\sigma^2} \exp\left[-\frac{(R-R')^2}{2\sigma^2}\right] \int_0^\pi \exp\left[\frac{RR'}{\sigma^2}(\cos\theta - 1)\right] d\theta\, RdR \tag{C4}$$

where θ is the angle between $\mathbf{R}$ and $\mathbf{R}'$. Hence

$$P(R|R') = \frac{R}{\sigma^2} \exp\left[\frac{-(R-R')^2}{2\sigma^2}\right] \left[\exp\left(\frac{-RR'}{\sigma^2}\right) I_0\left(\frac{RR'}{\sigma^2}\right)\right] \tag{C5}$$

where I_0 is the modified Bessel function of order zero. The probability P generated by a PSF involving several Gaussian components is the suitably weighted sum of expressions of the form of (C5).

For sufficiently small Δt the probability densities $\phi(R)$ and $\psi(R)$ become proportional to the observed and true surface brightnesses $\tilde{\Sigma}(R)$ and $\Sigma_t(R)$ at R. One may, in fact, identify ϕ and ψ with

$$\phi(R) = R\tilde{\Sigma}(R) \tag{C6}$$

$$\psi(R) = R\Sigma_t(R). \tag{C7}$$

A point source at the centre may be incorporated into this scheme by artificially enhancing the surface brightness interior to some very small radius.